

Evaluating the stress intensity factor for R350HT rail steel in relation to microstructure parameters

Sylwester Żak¹, Grzegorz Junak², Dariusz Woźniak³, Artur Żak³, Bartosz Chmiela²,
Magdalena Barbara Jabłońska⁴

¹ ArcelorMittal Poland S.A. Branch in Dąbrowa Górnicza, Aleja Józefa Piłsudskiego 92, 41-303 Dąbrowa Górnicza, Poland

² Faculty of Materials Engineering, Silesian University of Technology, Zygmunta Krasińskiego 8, 40-019 Katowice, Poland

³ Center for Metallurgical Technologies, Łukasiewicz Research Network - Upper Silesian Institute of Technology, ul. Karola Miarki 12-14, 44-100 Gliwice, Poland

⁴ Center for Advanced Material Technologies, Łukasiewicz Research Network - Institute of Non-Ferrous Metals, Sowińskiego 5, 44-100 Gliwice, Poland

* Corresponding author's e-mail: magdalena.jablonska@imn.lukasiewicz.gov.pl

ABSTRACT

The study highlights the advancement of rail transport, focusing on the distinct requirements of high-speed passenger transit and robust freight operations. Passenger rails emphasize geometric precision, such as straightness and minimal dimensional deviation, to reduce vibrations and improve safety and comfort. Freight rails, in contrast, require exceptional durability to withstand high axial loads, plastic deformation, and abrasive wear due to heavy tonnage. A key parameter for all rail types is the stress intensity factor (K_{Ic}), which ensures rail integrity by preventing crack propagation. The study confirmed that tested rail types (60E2 (rail profile, mass per meter 60.03 kg/m), 54E4 (rail profile, mass per meter 54.31 kg/m), and 49E1 rail profile, mass per meter 49.39 kg/m)) meet the EN 13674-1 standard for mechanical properties, indicating effective heat treatment. Residual stress levels were found to be low, particularly in lighter rails, enhancing resistance to brittle fracture. All rails exhibited a fine, fully pearlitic microstructure with cementite lamellae spacing between 92 and 106 nm, contributing to mechanical strength and durability. The low residual stress and high K_{Ic} (stress intensity factor, $\text{MPa}\cdot\text{m}^{1/2}$) support extended rail life and safety, as larger critical crack sizes minimize fracture risk. These findings underline the reliability and safety of rail materials under operational conditions, with consistent pearlitic structures and optimized stress properties ensuring robust performance.

Keywords: microstructure, strain, stress intensity factor, heat treatment, rail steel, pearlite, interlamellar spacing

INTRODUCTION

Current trends in the development of rail transport can be divided into two separate areas, which impose different requirements on the properties of rails. These are high-speed tracks for passenger transport vehicles and tracks for freight transport [1]. Freight transport have different requirements, as they must carry high axial and total loads, and the transported tonnage is over $50 \cdot 10^6$ Mg gross per year [2].

For rails intended for passenger transport, the geometric features of the rails are important, such as minimum dimensional deviations of the cross-section parameters, especially the width of the rail head, the running surface, asymmetry, and the height of the rail [1, 2]. For this application, it is also essential to ensure the proper straightness of the rails measured along the length of the rail and at its ends. The European standard EN 13674-1 [3] specifies very rigorous conditions for rail straightness, defining the maximum deviation of

straightness in the vertical plane at 0.3 mm over a measuring length of 3 m, so the special requirements for straightness are the result of the need to reduce the amplitude of vibrations in the vertical plane of the rail during track operation. Too many deviations from straightness can initiate vibrations leading not only to a decrease in ride comfort but also to damage to rail vehicles and the track [4].

Modern rails, regardless of their purpose, should be characterized by high metallurgical purity and an appropriate level of plastic and mechanical properties, including hardness and resistance to brittle fracture expressed by the stress intensity factor K_{Ic} , which is a material feature that determines its susceptibility to uncontrolled crack development and, consequently, rail fracture [4]. An appropriately high level of impact strength and a low level of residual stresses are also important [5, 6]. Rails intended for the transport of goods should be characterized by high resistance to plastic deformation and abrasive wear as well as low susceptibility to the formation of contact-fatigue defects, i.e. maintaining a balance between wear due to abrasion and contact fatigue [13].

There is a correlation between the stress intensity factor, the stress level in the rail, and the critical crack length [7]. The total stress in the rail is the sum of the residual stress σ_E (residual stress, MPa), the thermal stress σ_T (thermal stress, MPa) ranging from -125 MPa to +125 MPa and the stress resulting from the operational stress σ_v , which can reach a value of up to 200 MPa [7]. The relationship between the transferred stress and the crack length

at the assumed constant stress intensity factor K_{Ic} equal to $31 \text{ MPa}\cdot\text{m}^{1/2}$ is shown in Figure 1.

Assuming that the longitudinal tensile stress in the rail foot is 250 MPa, the thermal stress value is 50 MPa and the stress from rail bending during operation is 200 MPa, according to Figure 1, a defect with a depth of 1.2 mm will already cause the rail to crack – case A (elongation, %). If the residual stresses in the rail were reduced by half to 125 MPa, the critical crack length would increase to about 2.3 mm – case B. Assuming that the value of operational stress is 100 MPa, with a constant thermal stress of 50 MPa and the rail residual stress of 250 MPa and 125 MPa. Respectively, the critical crack length would be 2 mm for case C and 10 mm for case D. Since in practice there is no effect on thermal and operational stresses, reducing the residual stresses in the rails and increasing the stress intensity factor means improving the reliability of the rails and increasing the safety of rail transport. In addition, safety is improved by the fact that longer cracks are easier to detect during flaw detection tests, which reduces the probability of failure to detect a developing crack in the rail in time and, as a result, a fracture. The reduced level of residual stresses also results in a reduction of the average value of operating stresses, which in turn slows down the development of a crack. Additionally, contact-fatigue defects such as shelling, head checking, squats, and others can develop in the rail head, which often lead to a rail fracture. To counteract the development of

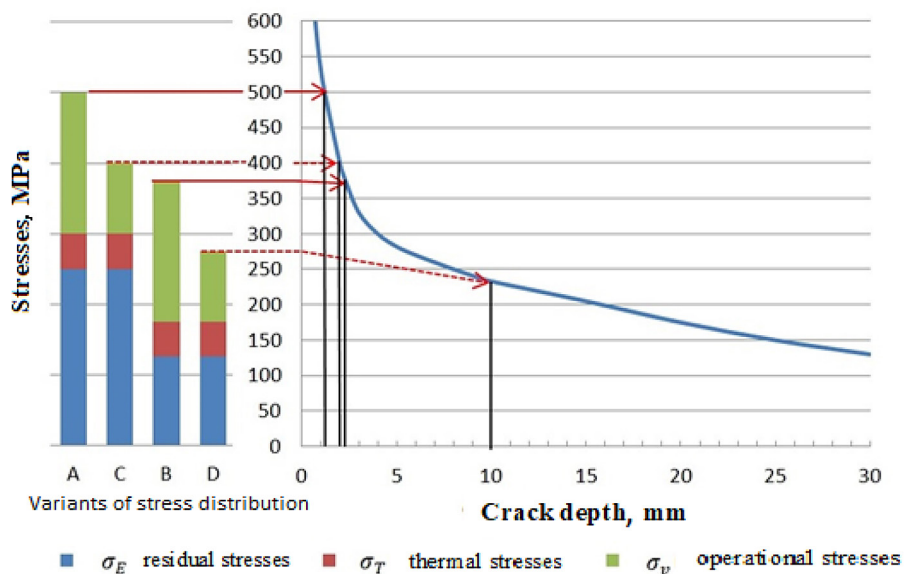


Figure 1. Dependence of the critical crack length on the tensile stress. own study based on [7]

these defects, the lowest possible level of tensile stresses in the rail head is desirable. If the tensile stresses reach a critical value of the stress intensity factor K_{Ic} (determining the resistance to brittle fracture), the crack develops in an uncontrolled manner leading to a rail fracture [4].

The basic document that describes the requirements for rails is the European standard EN 13674-1 [3]. It indicates the strain gauge method for assessing the level of stresses in rails as part of product qualification tests. Residual stresses in rails are measured in the centre of the bottom surface of the foot using the cutting method. This method allows the determination of longitudinal stresses.

REQUIREMENTS FOR HEAT TREATED RAILS

The basic grade of rail steel widely used to produce rails is the R260 grade, with hardness defined at the level of 260–300 HBW. This is a steel grade that is not heat treated, so the rail properties are obtained as a result of natural cooling of the rails from finish rolling temperature. To obtain a much higher level of hardness, heat treatment of the rail head is used. It increases the hardness on the running surface to the level of 350–390 HBW for grade R350HT [3]. The difference in the chemical composition of both steel grades is small, the only significant difference is the increase in the lower carbon content for grade R350HT from 0.62 to 0.72% by weight [3]. However, it is important to increase the level of mechanical properties by heat treatment of the R350HT grade [3]. This is achieved by modifying the morphology of pearlite [1], especially by reducing the spacing between cementite lamellae in pearlite and changing the thickness of cementite lamellae [8], but also by reducing the average size of austenite grains [9]. This can be achieved in two ways, the first one involves modifying the chemical composition by adding elements such as: Cr, V, Ti, Nb, Mo, Ni which have a beneficial effect on the structure and increase the level of mechanical properties of pearlitic steels without the need for heat treatment [10, 11]. Another possibility is heat treatment [29] applying one of the cooling media used: compressed air, water-air spray or a water-polymer mixture [9]. There are also studies describing the yield strength using the Hall–Petch relationship in fully pearlitic steels, replacing the average grain size with the spacing between cementite lamellae in pearlite such as in

the manuscripts of the Sevillano [18] and Ray and Mondal [19]. For comparison, one can also cite the results of tests for B1000 grade steel presented in [1]. The strengthening of this steel is a result of modification of the chemical composition by using V and Cr additives, and the rails produced with this grade were cooled naturally using the same cooling rate as for raw rails, i.e. without the use of accelerated cooling. The following property levels were obtained: hardness in the range of 334–359 HBW, average austenite grain size 46.5 μm , average value of the stress intensity factor measured on 5 specimens was 36.36 $\text{MPa}\cdot\text{m}^{1/2}$. The chemical composition of grade B1000 for which the results were presented was as follows: C=0.80%, Mn=1.15%, Si=0.47%, Cr=0.50%, V=0.054%, P=0.018%, S=0.010%, Al=0.004%. The study [11] presented the results of tests for tram rails manufactured with B1000 grade steel, the hardening of which was also obtained by modifying the chemical composition. The paper [20] described the mechanical properties of steel with an almost fully pearlitic structure, with a carbon content of 0.65% C, as a function of interlamellar spacing. It was noted that below the critical value of this spacing UTS, impact strength and ductility do not change significantly. However, none of the studies [1, 10, 11] provides the value of the spacing between cementite lamellae in pearlite. The above examples show that despite the use of different steel hardening mechanisms (heat treatment or modification of the chemical composition), a similar level of hardness is obtained on the running surface of the rail head, and the range of results obtained for the stress intensity factor K_{Ic} is also similar. In the literature, numerous attempts have been made to determine the relationship between the morphology of the microstructure [12] and the operational properties of rail steel [13]. Based on studies conducted using X-rays with synchrotron radiation [27] and the neutron diffraction method [19], it was established that for a structure consisting of 100% pearlite, the properties of steel depend on the shape of cementite, grain size and, above all, the spacing between cementite lamellae in pearlite (Sp).

In the case of heat treatment of railway steels, relevant information dates back to the 1970s, especially regarding cooling methods. Reducing the spacing between cementite lamellae in pearlite increases the strength and hardness of the pearlite structure, which directly improves the wear resistance of the railhead running surface. Various

accelerated cooling methods have been described in the literature, including the use of water [30, 31], water-air mist [32], compressed air [31, 33], and immersion in aqueous polymer solutions [9, 33]. However, most manuscripts present general solutions without describing in detail the correlation between the spacing between cementite lamellae in pearlite, cooling rate, and mechanical properties. This specific information is particularly lacking, especially for R350HT steel. Furthermore, from the point of view of a complete analysis, it is also important to describe and analyze qualitatively, but also quantitatively, the fractures resulting from fatigue fracture, which allows one to reflect on and explain in detail the fracture mechanisms accompanying crack development. Such research was carried out, for example, in the paper [34], where quantitative fractographic analysis was performed to reconstruct the fracture events using the complementary fracture surfaces of a failed specimen or a mechanical component as FRacture Surface Topography Analysis (FRASTA). Similar research was conducted in a paper [35] where the authors made a qualitative and quantitative description of the fracture mechanism on the example of tests performed for chromium-molybdenum steel and proposed a model for predicting the fatigue life of the material, based on the whole fracture surface method.

This article aims to analyze the relationship between the chemical composition, processing parameters, and key mechanical properties, specifically the K_{Ic} coefficient and the interlamellar spacing in pearlite colonies. The study correlates the results of stress intensity factor tests with the pearlite morphology, characterized by

the austenite grain size and the spacing between cementite lamellae. The tests were conducted on various rail profiles, including light rail type 49E1, medium rail type 54E4, and heavy rail type 60E1, used in different operational track applications.

MATERIAL FOR TESTING

The material for the tests was R350HT rail steel with a chemical composition, according to the melt analysis, given in Table 1, compliant with the requirements of the EN 13674-1 standard [3]. The test specimens came from rails heat treated according to the developed technology, manufactured in the heavy-section mill of ArcelorMittal Poland S.A. using accelerated rail head cooling in a water-polymer mixture. Since the range of chemical composition for each melt (“heat” according to the nomenclature used in the standard [3]) was maintained in a very narrow range for all elements, it can be assumed that the material was homogeneous and the influence of the chemical composition on the obtained results can be ignored.

EN 13674-1 [3] standard requires the determination of the minimum value of a single stress intensity factor result and its minimum average value during qualification tests. According to the standard, tests are carried out on the heaviest type of rail produced, in the case of AMP on the 60E1 (60E2) rail. In this study specimens from three types of rails were used, i.e. the heaviest 60E1 profile with a mass of 60.21 kg/m, the average in terms of mass 54E4 profile, the theoretical mass of which is 54.31 kg/m and the relatively light 49E1 rail with a mass of 49.10 kg/m. The above

Table 1. Chemical composition of individual melts

Marking	Mass in liquid state, %									10 ⁻⁴ %, ppm	
	C	Mn	Si	P	S	Cr	Al max	V max	N max	O max	H max
49E1 A402-13	0.78	1.13	0.38	0.010	0.019	0.08	0.003	0.002	0.0049	20	1.1
54E4 A104-12	0.77	1.08	0.39	0.009	0.014	0.08	0.004	0.001	0.0054	18	1.3
60E2 A502-8	0.77	1.07	0.35	0.008	0.016	0.08	0.004	0.001	0.0055	18	1.8

Table 2. Basic properties of the tested rail steel for individual rail types

Specimen marking	Basic mechanical properties				
	Tensile strength, R_m , MPa	Yield strength, $R_{p0.2}$, MPa 20°C	Elongation, A_5 [%]	Hardness, HB	Residual stresses MPa
49E1-A402-13	1270	869	10.2	378	52
54E4-A104-12	1230	841	9.5	363	87
60E2-A502-8	1265	845	9.5	365	98

for conducting the process. Table 3 shows the applied heat treatment parameters, while Table 4 compares the hardness measurements at individual points on the rail head cross-section in accordance with Figure 2 and the measured hardness in the fatigue zone of the fracture. The starting point for the selection of parameters was a comparison of the rail head surface area for individual profiles. According to the calculated values of the rail head surface area, which amount to:

- 49E1 – 29.82 cm² (rail head width 67 mm, height 51.5 mm),
- 54E4 – 31.90 cm² (rail head width 67 mm, height 55 mm),
- 60E1 – 30.84 cm² (rail head width 72 mm, height 51 mm).

The difference in the surface area of the rail heads is 2.08 cm², which should be considered a rather insignificant value. It can be assumed that similar values of the geometric parameters of the rail heads 49E1, 54E4, and 60E1 translate into similar values of the surface area, and thus into a very similar value of the accumulated heat in the rail head of a given type, which ensures similar conditions for the pearlitic transformation during the heat treatment of the rail profiles in question.

The static tensile test is performed by EN ISO 6892-1 [24] using a 10 mm diameter specimen. Before the test, the tensile strength test specimens should be heated at 200 °C for up to 6 hours. The methodology for measuring residual stresses described in Section 8 Qualification tests and Annex C of the standard [3] includes the following assumptions: residual stresses in rails are measured in the middle of the lower surface of the foot using the cutting method. It consists of sticking a strain gauge on the surface of the test specimen and cutting it near the attached strain gauge; during cutting, the rail should be cooled. The thickness of the cut rail slice is 20 mm. As a result of cutting, deformations occur in the longitudinal and transverse directions, related to the residual stresses. The residual stresses are calculated based on the differences between the first and second set of measurements of released deformations by multiplying by the Young’s modulus constant of $2.07 \cdot 10^5$ MPa. According to the standard, the maximum longitudinal residual stress in the foot should be 250 MPa for all steel grades.

The fracture toughness tests were carried out on the MTS-810 servo-hydraulic testing machine (Fig. 3) on specimens for three-point bending (Fig. 4). The method of supporting the



Figure 3. Generating a pre-fatigue crack

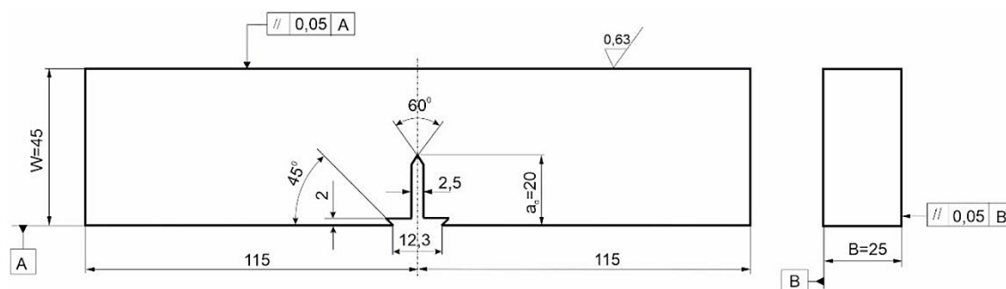


Figure 4. Specimen for testing fracture toughness under three-point bending conditions

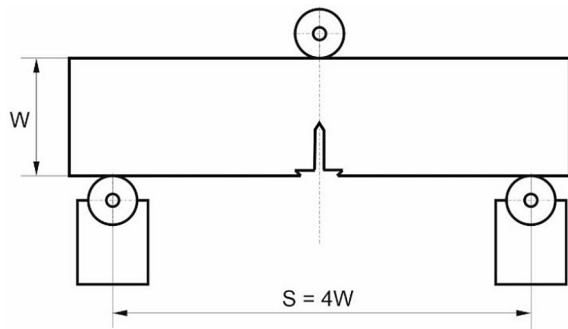


Figure 5. Method of supporting the specimen under fracture toughness testing conditions

specimen during the tests is shown in Figure 5. The tests were carried out in accordance with the standards: PN-EN 13674-1: Vingole railway rails with a mass of 46 kg/m and more [3] and ISO 12108:2018 [25].

The fatigue crack was generated at room temperature, and the fracture of the specimens with the generated crack was performed at -20 °C, exactly as indicated in the standard [3].

The fatigue crack was generated in the initial phase of the process on the MTS-810 servo-hydraulic testing machine at the force range of 50 kN under the conditions of repeating-stress cycle ($R=0.1$), with the parameters as shown in Table 5. The load change frequency during crack generation was $f=5$ Hz (f – load frequency, Hz). In the final stage of crack generation, when the fatigue crack in the tested specimens reached half of the required length ($a_s \cong 1$ mm), the loads P_{min} and P_{max} were reduced to the values shown in Table 6. Therefore, the conditions for crack generation specified in EN 13674-1 [3] and ASTM E399 [26] were met.

$$K_{fmax} = P_Q \times \frac{S}{B \times W^{\frac{3}{2}}} \times f \left(\frac{a}{W} \right) \times 0.031623; [MPa \cdot m^{1/2}] \quad (1)$$

For the determined K_{Ic} value to be compliant with the standards, the conditions for generating a fatigue crack must be met:

$$W1. K_{fmax}/E < 0.00032 [m^{1/2}] \quad (2)$$

$$W2. \Delta K_f \leq 90\% K_{fmax} [MPa \cdot m^{1/2}] \quad (3)$$

Then, the specimen with the generated crack was subjected to static bending on the MTS-810 testing machine at a force range of 100 kN. The test was carried out until fracture.

Based on the recorded graph, the value of the force P_Q and F_{max} was determined. On the obtained specimen fractures, the fatigue crack length (a_s) was measured, as well as the total crack length a , i.e. with the mechanical notch a_o ($a = a_o + a_s$), measured at $1/4$, $1/2$ and $3/4$ of the specimen thickness. Then, fractographic analysed of the fractures were performed. The studies were carried out using the scanning electron microscopy (SEM) method using a HITACHI S-3400N scanning microscope equipped with an electron gun with a tungsten fiber operating at an accelerating voltage of 30 kV. The microstructure was analysed by light microscopy using an Olympus GX51 microscope. The measurements of the interlamellar spacing in pearlite were performed using two methods, which were also used in [21]. There are several methods of measuring the spacing between cementite lamellae in pearlite in the literature, two of which seem to be the most convenient. The first one is the *CLM* method (circular line method) [17], which consists of placing the boundary of 3 pearlite colonies in a circle of a given diameter and determining the number of intersections of the cementite lamellae with the circle, and the *LIM* (linear intersection method) [18]. In order to describe the microstructure morphology more precisely, the characteristic features should be defined appropriately. When measuring the interlamellar spacing of pearlite, it is important to take into account the fact of the uniform distribution of pearlite in the entire material [20].

Table 5. Parameters of fatigue crack generation in the initial phase in R350HT steel specimens

Steel grade	P_{max} [N]	P_{min} [kN]	Stress intensity factor $K_{f,max}$ [MPa·m ^{1/2}]	Frequency [Hz]
R350HT	14000	1400	22.9	5

Table 6. Parameters of fatigue crack generation in the final phase of the process

Steel grade	P_{min} [N]	P_{max} [N]	$K_{f,min}$ [MPa·m ^{1/2}]	$K_{f,max}$ [MPa·m ^{1/2}]	ΔK_f [MPa·m ^{1/2}]
R350HT	1200	12000	2.17	21.74	19.5

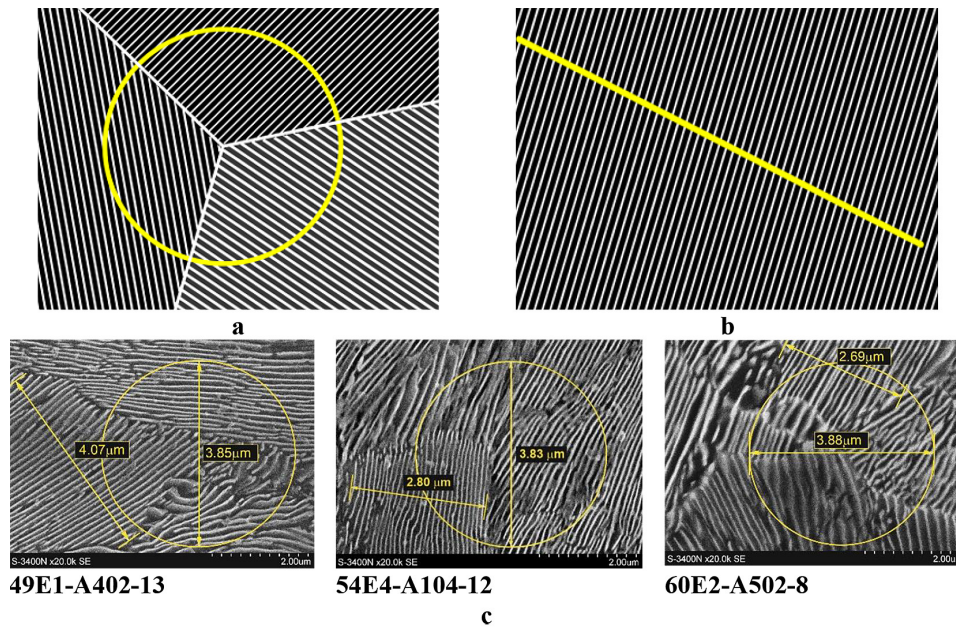


Figure 6. Schematic presentation of the interlamellar spacing measurement method in pearlite: (a) CLM [18] and (b) LIM [19], (c) example presentation of the CLM and LIM methods on real SEM images of the tested specimens

For the measurements, it is necessary to analyse the interlamellar spacing for the areas appropriate to the inclination of the pearlite lamellae to the observation plane (Fig. 6).

The study also analysed the size of the pearlite colony. Based on SEM images using the Inspect F scanning electron microscope from FEI. Microphotographs were taken at random locations on the transverse section taken from the foot and head of the experimental rail sections. The measurements of the size of the pearlite colony were performed using specialist computer software “μgrain” [22]. The program allows for determining the size of the pearlite colony based on measurement lines drawn through the boundaries of the pearlite colony. In order to determine

the size of the pearlite colony, the following relationship was used [14]:

$$dp = \frac{d1+d2}{2} \tag{4}$$

where: dp = pearlite colony size, μm ; $d1$ = maximum colony length, μm ; $d2$ = maximum colony width, μm

TESTS RESULTS

The method of determining KIC is presented in the following computational algorithm Figure 7. Figures 8, 9, 10 shows the recorded force-displacement relationships during the tests, based on which the P_Q and P_{max} force values were determined. The determined values were used in the

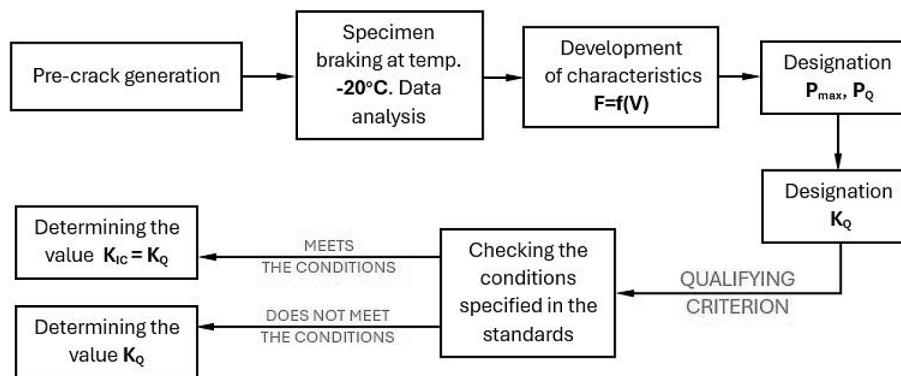


Figure 7. Computational algorithm of the method of determining KIC

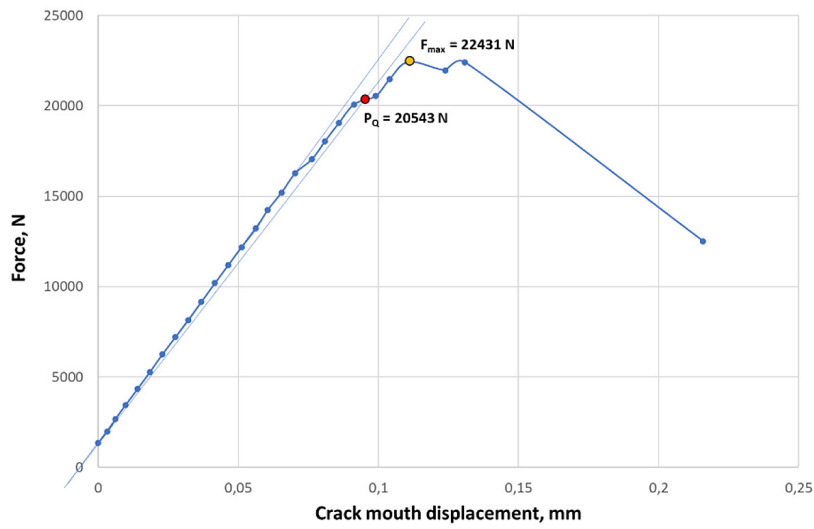


Figure 8. Force-displacement relationship for specimen 54E4-A104-12

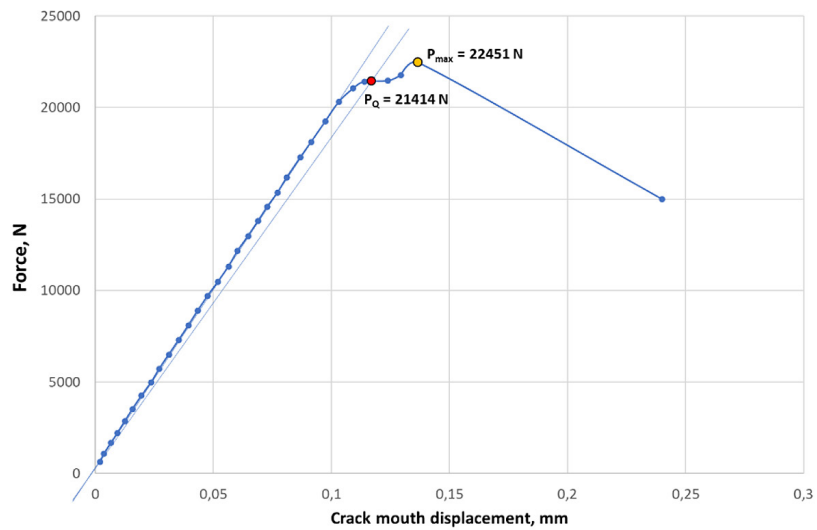


Figure 9. Force-displacement relationship for specimen 49E1-A402-13

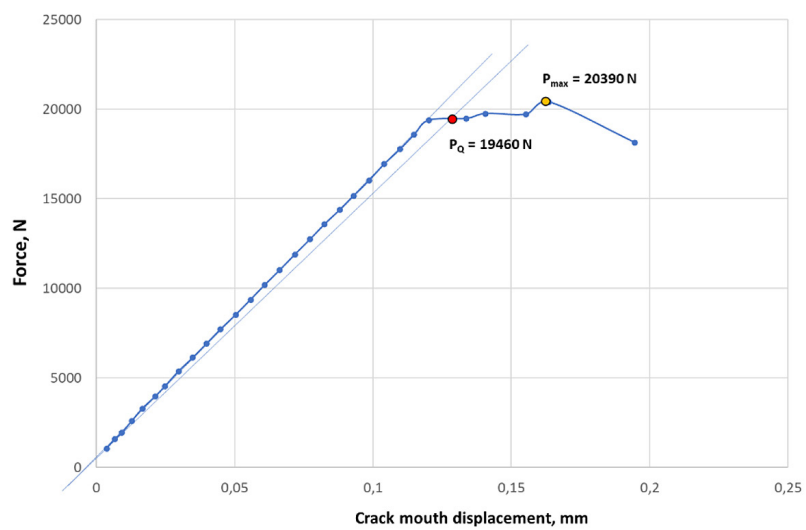


Figure 10. Force-displacement relationship for specimen 60E2-A502-8

Table 7. Summary of data for determining the calculated value of fracture toughness K_Q (crack length measurement results and force value P_Q) – R350HT steel.

Crack depth a_s and total notch measurement results $a = a_o + a_s$)			Measurements average, mm	P_Q , kN
1/4 B	1/2 B	3/4 B		
Specimen no. A402-13 $a_o = 19.5$ mm				
$a_s = 2.20$	$a_s = 2.11$	$a_s = 1.98$	$a_s = 2.10$	21.4
$a = 21.70$	$a = 21.61$	$a = 21.4.8$	$a = 21.60$	
Specimen no. A104-12 $a_o = 19.5$ mm				
$a_s = 1.93$	$a_s = 2.22$	$a_s = 1.88$	$a_s = 2.01$	20.5
$a = 21.43$	$a = 21.72$	$a = 21.38$	$a = 21.51$	
Specimen no. A502-8 $a_o = 20$ mm				
$a_s = 2.18$	$a_s = 2.38$	$a_s = 2.05$	$a_s = 2.20$	19.4
$a = 22.18$	$a = 22.38$	$a = 22.05$	$a = 22.20$	
a_o – length of the machined notch, a_s – length of the fatigue crack, a – total length of the crack.				
NOTE: static bending (breaking) of specimens at temperature -20 °C.				

calculations of fracture toughness. It can be seen that the characteristics show a similar trend during the static bending test. In each case, the condition $P_{max}/P_Q \leq 1.1$ was met, as shown in Table 7.

Fracture toughness calculation results

The obtained data were used to were used to calculate the value of fracture toughness K_Q (stress intensity factor, $\text{MPa}\cdot\text{m}^{1/2}$) (Table 8) using the relationship [15]:

$$K_Q = \frac{P_Q}{B \cdot W^{1/2}} \times g\left(\frac{a}{W}\right) \times 10^{1.5} \quad (5)$$

Table 8. Summary of the calculation results of the fracture toughness of R350HT steel

Specimen marking	P_Q [N]	K_{Ic} (K_Q) [$\text{MPa}\cdot\text{m}^{1/2}$]
49E1-A402-13	21 414	40.4
54E4-A104-12	20 543	38.4
60E2-A502-8	19 460	38.1

$$g\left(\frac{a}{W}\right) = \frac{6\alpha^{0.5}}{\left[(1 + 2\alpha)(1 - \alpha)^{3/2}\right]} \quad (6)$$

$$\left[1.99 - \alpha(1 - \alpha)(2.15 - 3.93\alpha + 2.7\alpha^2)\right] \quad (7)$$

$$\alpha = \frac{a}{W}$$

The material resistance to cracking in a plane strain state K_{Ic} corresponds to the K_Q value if the conditions specified in Tables 9, 10 and 11 are met. For the tested rail sections of different profiles, the stress intensity factor values obtained ranged from $38.0 \text{ MPa}\cdot\text{m}^{1/2}$ to $40.4 \text{ MPa}\cdot\text{m}^{1/2}$. Table 12 presents a summary of the stress intensity factor test results.

These are similar to those given in [9], where the given ranges of stress intensity factor values tested on heat-treated rail specimens are within the range of $37\text{--}42 \text{ MPa}\cdot\text{m}^{1/2}$. The values of the conventional yield strength $R_{p0.2}$ determined at a temperature of -20 °C were assumed to calculate the K_{Ic} value.

Figures 11–12 show the microstructure of the specimens tested according to the methodology described in point 4.

Table 9. Conditions checking

Specimen	Conditions checking	
	$a \geq 2.5 \times \left(\frac{K_Q}{R_{p0.2}}\right)^2 \cdot [\text{m}]$	$B \geq 2.5 \times \left(\frac{K_Q}{R_{p0.2}}\right)^2 \cdot [\text{m}]$
Marking	Steel– R350HT	
49E1-A402-13	0.0216 > --- 0.0055	0.0250 > --- 0.0055
54E4-A104-12	0.0215 > --- 0.0052	0.0250 > --- 0.0052
60E2-A502-8	0.0222 > --- 0.0051	0.0250 > --- 0.0051

Table 10. Conditions checking

Specimen	Conditions checking
	$(W - a) > 2.5 * \left(\frac{K_Q}{R_{p0.2}} \right)^2, [m]$
Marking	Steel – R350HT
60E2-A502-8	0.0228 > --- 0.0051
54E4-A104-12	0.0235 > --- 0.0052
49E1-A402-13	0.0234 > --- 0.0055

Table 11. Conditions checking $F_{max}/P_Q \leq 1.1$

Specimen marking	P_Q [N]	P_{max} [N]	P_{max}/P_Q
49E1-A402-13	21414	22451	1.05
54E4-A104-12	20543	22431	1.09
60E2-A502-8	19460	20390	1.05

Microstructure analysis

The microstructure of the tested steels is pearlite, the morphology of which is shown in Figure 11. The results of the quantitative analysis of pearlite colonies indicate that the size of the colonies in the rail head for all tested specimens

is within the range of 2.39 μm to 9.01 μm , which is consistent with the microstructure observations, where in specimen 60E2 the occurrence of pearlite colonies with a more diverse size was observed than in the case of the other profiles (Fig. 12). Considering the average values of the obtained results of the pearlite colony size, it can be seen that the average size of the pearlite colony for specimen 60E2-A502-8 is 5.87 μm . for specimen 54E4-A104-9 it is 5.44 μm and for specimen 49E1-A402-13 it is 5.48 μm . This size is referred to the ASTM E112 standard [15] according to which the grain number of former austenite is from 5.0 to 5.5 – Table 13.

As can be seen in the fatigue scrap area, the generation of crack does not affect the degradation of pearlite lamellae. Morphologically, pearlite is very fine.

Its average inter-lamellar spacing for all tested specimens does not exceed 100 nm. The results of inter-lamellar spacing calculations are given in Table 14. Comparing the results obtained in these studies, for example in [8] the ranges of austenite grain size in raw steel were defined at 100–200

Table 12. Summary table. summary of the final results of the study – R350HT

Specimen marking	$R_{p0.2} (-20 \text{ }^\circ C)$ MPa	$K_{Ic} [K_Q]$ MPa m ^{1/2}	Average $K_{Ic} [K_Q]$ MPa m ^{1/2}	Standard dev. MPa m ^{1/2}
60E2-A502-7	840	39.9	39.8	1.35
60E2-A502-8		38.1		
60E2-A502-9		41.4		
49E1-A402-11	860	38.2	38.9	1.09
49E1-A402-13		40.4		
49E1-A402-16		38.8		
54E4-A104-8	843	39.7	38.7	0.74
54E4-A104-9		38.0		
54E4A104-12		38.4		

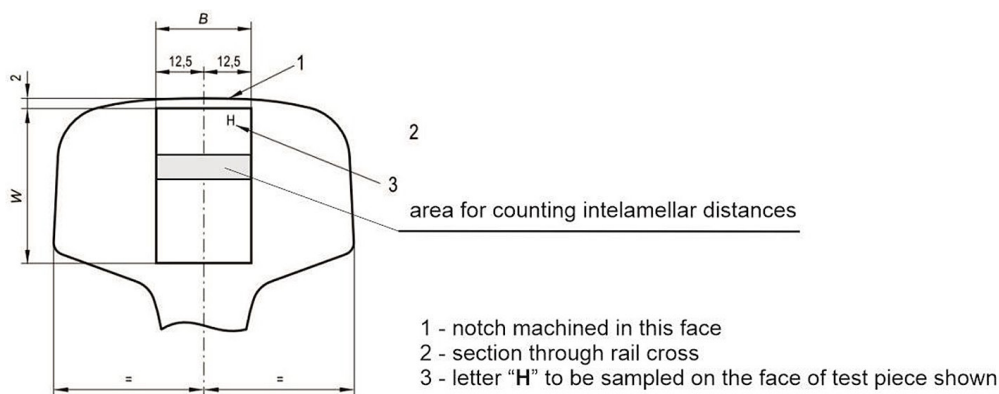


Figure 11. Interlamellar spacing calculation area

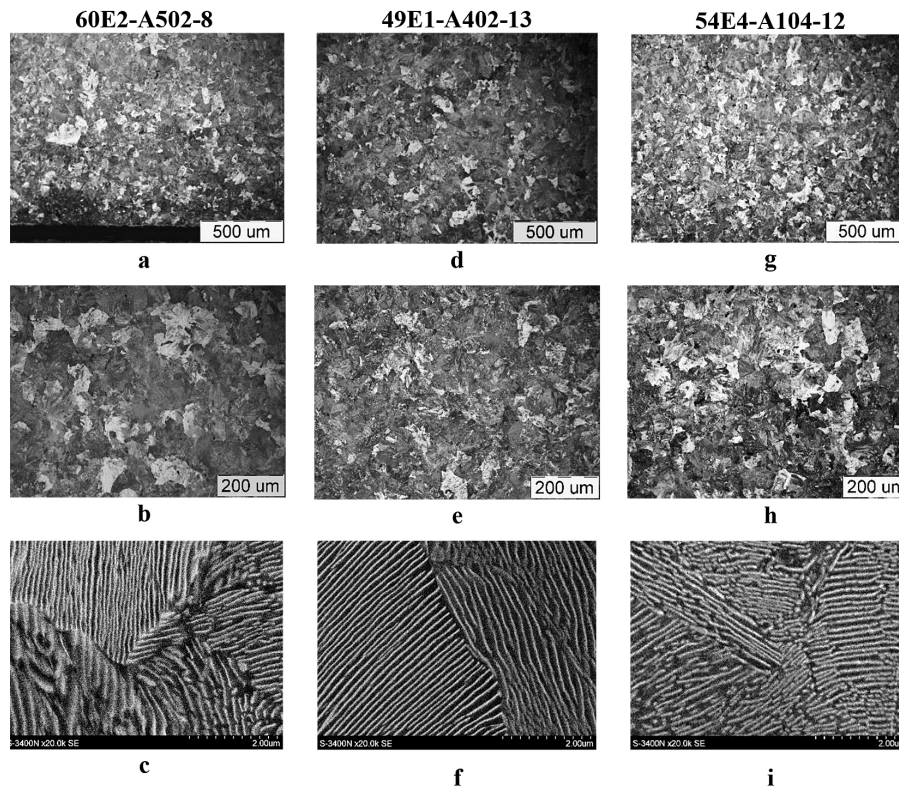


Figure 12. Microstructure at the fatigue scrap location a, b, d, e, g, h) L, c, f, i) SEM

Table 13. Measurement results of pearlite colony size and former austenite grain size in the rail head

Specimen marking	Pearlite colony size in the rail head, μm	Average pearlite colony size in the rail head, μm	Mean grain chord, μm	Grain No. acc. ASTM E112
49E1-A402-13	2.39–8.56	5.48	47.24	5.5
50E4-A104-12	3.17–7.70	5.49	56.30	5.0
60E2-A502-8	2.73–9.01	5.87	48.36	5.5

Table 14. Average values of the calculated interlamellar spacing of perlite

Specimen marking	S1, nm (CLM method)	S2, nm (LIM method)
49E1-A402-13	67.99	99.80
54E4-A104-12	78.22	102.90
60E2-A502-8	64.14	92.12

μm , and for heat-treated steel 20–25 μm . On the other hand, the inter-lamellar spacing was defined at 0.20–0.25 μm for raw steel, and for heat-treated steel in the range of 0.09–0.12 μm .

In turn, in the article [9] for heat-treated rails, where the immersion method in a water-polymer mixture was used. the measured value of the spacing between cementite lamellae in pearlite colonies was in the range of 0.07–0.11 μm , and the average size of pearlite colonies was

6.3 μm . These tests were performed on rail steel with the following chemical composition: melt 811 – content C=0.73%, Mn=1.25%, Si=0.27%, P=0.006%, S=0.013%, Al <0.005%; melt 814 – content C=0.73%, Mn=1.01%, Si=0.28%, P=0.006%, S=0.011%, Al <0.005%.

The results obtained for the tested rail sections of different profiles indicate that the inter-lamellar spacing was 0.06 μm to 0.11 μm with a pearlite colony size of less than 6 μm . This indicates the use of well-selected railhead cooling parameters for all tested profiles in industrial conditions.

All quantitative results of fatigue zone depth measurements both at the edges and in the central zone indicate that one of the conditions for generating a fatigue crack was met [3]. The results of fractographic tests are presented in Figures 13–16. It was found that the fatigue fracture surfaces exhibited the typical mechanisms

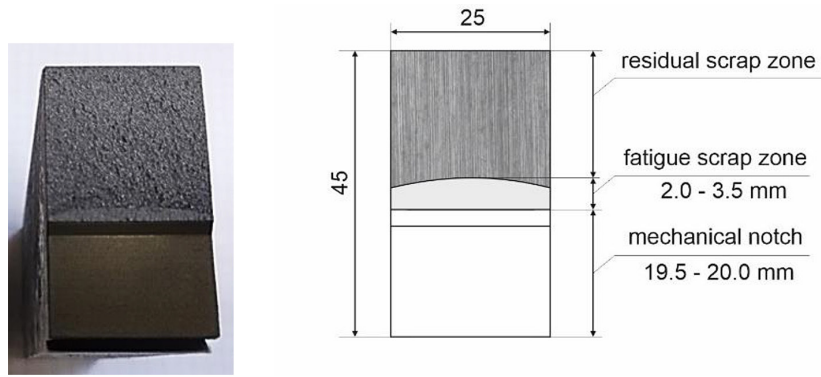


Figure 13. Schematic representation of the fractographic observation area

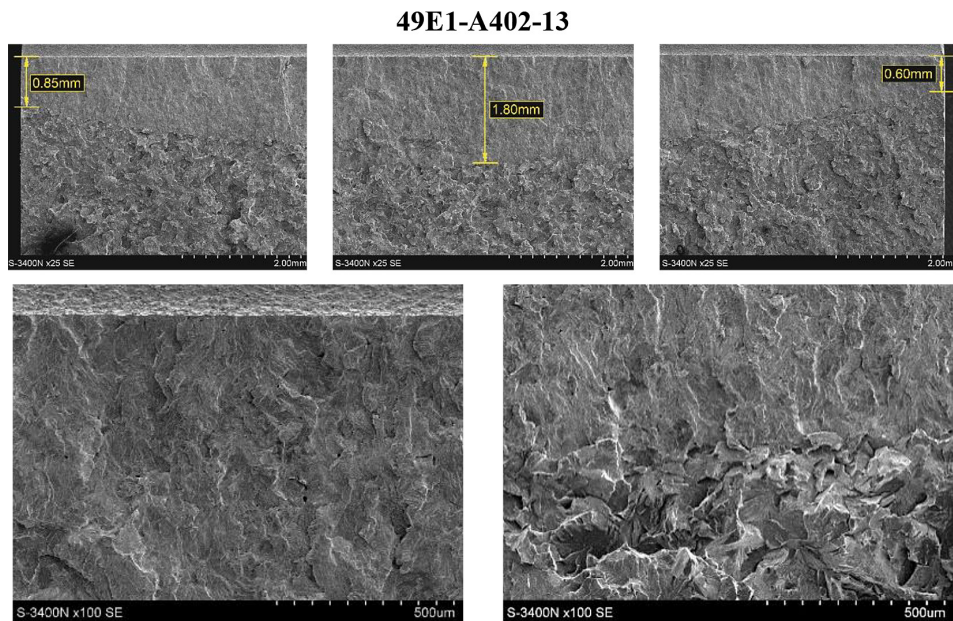


Figure 14. Microstructure of the fatigue zone area for the 49E1 type rail (SEM)

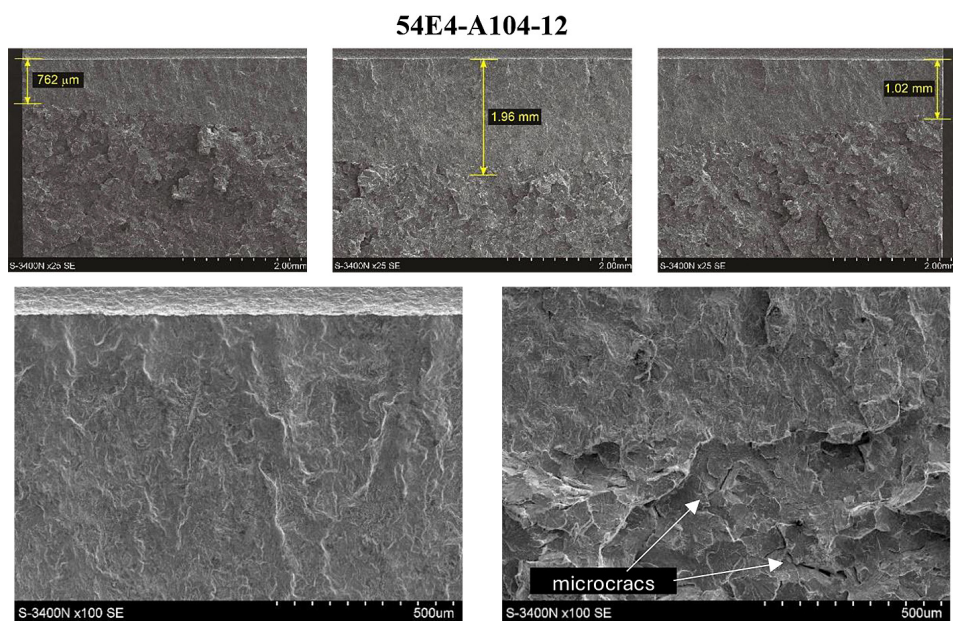


Figure 15. Microstructure of the fatigue zone area for the 54E4 type rail (SEM)

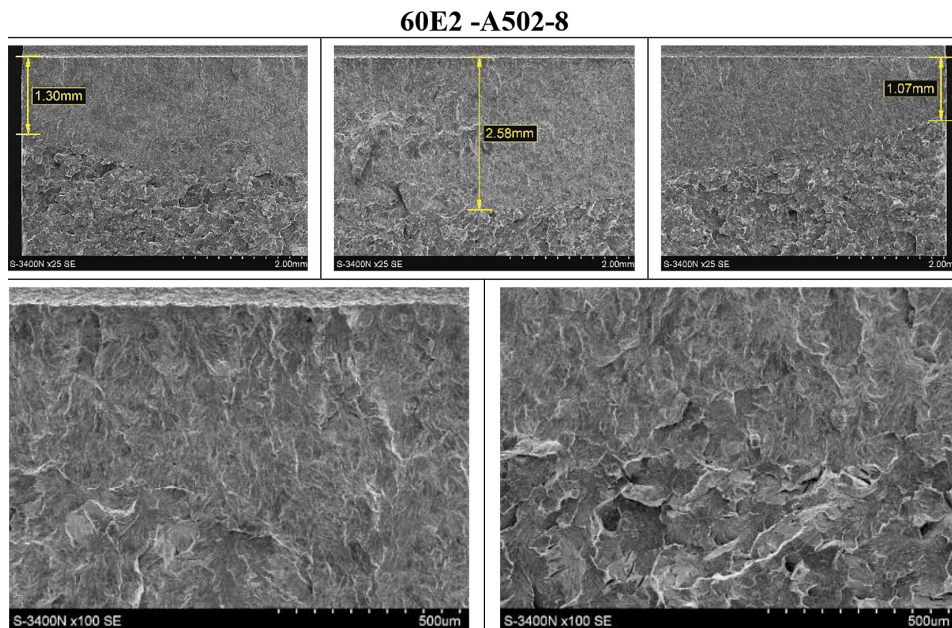


Figure 16. Microstructure of the fatigue zone area for a 60E2 type rail (SEM)

associated with the fatigue failure of metallic materials. The fractures have river patterns, traces of plastic deformation, cleavage facets. Was not observed there a ductile dimples. No microcracks were observed in the fatigue fracture area on the specimens from profiles *49E1* and *60E2* (Fig. 14 and Fig. 16). Microcracks occurred only for profile *54E4* (Fig. 15), and they were of a single character.

CONCLUSIONS

The results obtained for each type of rail, i.e. heavy *60E2*, medium *54E4* and light *49E1*, with regard to the basic mechanical properties R_m , $R_{p0.2}$, A . and a hardness and, mainly, the analysed in this study, meet the requirements of EN 13674-1. It indicates that the heat treatment technology was properly developed.

The determined values of the stress intensity factor were in the range of 38-40 $\text{MPa}\cdot\text{m}^{1/2}$ and their average value was for *49E1* 38.9 $\text{MPa}\cdot\text{m}^{1/2}$, for *54E4* 38.7 $\text{MPa}\cdot\text{m}^{1/2}$ and for *60E2* 39.8 $\text{MPa}\cdot\text{m}^{1/2}$, respectively. Such values confirm the high fracture toughness of the steel, which is much higher than the minimum value of 32 $\text{MPa}\cdot\text{m}^{1/2}$ specified in EN 13674-1.

It should be emphasized that the levels of residual stress measured by the tensometric method in the rail foot were low, for the *60E2* profile only 98 MPa, i.e. more than two and a half times lower

than the requirements of the standard EN 13674-1 set at 250 MPa. In the lighter types of rails *54E4* and *49E1*, the measured stress level was even lower, amounting to 87 MPa and 52 MPa, respectively. This is a very good prognosis for the rails operating properties, and especially their resistance to brittle fracture.

The microstructure for each type of rail tested was fully pearlitic with a fine-lamellar microstructure, where the measured spacing between cementite lamellae in pearlite was from 92 nm to 106 nm. This indicates a high degree of pearlite refinement, which affects the obtained level of mechanical properties regardless of the grain size of former austenite measured by the size of pearlite colonies. It should also be noted that no unacceptable bainitic or martensitic structures were observed in the rails.

The resulting combination of low residual stress and high stress intensity factor K_{Ic} for each type of rail is very beneficial from the point of view of rail service life. This ensures an exceptionally high value of the critical crack size, i.e. the size of the defect that will cause the rail to crack. This will directly translate into increased reliability of heat-treated rails, and consequently safety in rail traffic in all operating conditions.

The measured pearlite colony size range and the average pearlite colony size for all rail types are at the same level between 5.87–5.48 μm , a slight increase in the mean grain chord value was observed for the *54E4* rail compared to the other

rail types, which resulted in a smaller grain size for this specimen.

The inter-lamellar spacing calculated using the circular line method (*CLM*) and the linear intersection method (*LIM*) for rails *60E2* and *49E1* were at a similar level, for *49E1*, 67.99 nm (*CLM*) and 99.80 nm (*LIM*), for *60E2*, 64.14 nm (*CLM*) and 92.12 nm (*LIM*). Only a slight increase in the inter-lamellar spacing was noted for rail *54E4*, 75.15 nm (*CLM*), and 106.23 nm (*LIM*), which indicates slightly lower refinement of the pearlitic structure in the tested area.

The evaluation of fractures in the fatigue region indicated the presence of a ductile fracture with brittle elements as evidenced by single microcracks observed only in specimen *54E4*.

Due to the similar values obtained between the cementite lamellae in pearlite for each type of rail, the calculated average values of the stress intensity factor for each type of rail are also at the same level. It can therefore be concluded that for the inter-lamellar spacing of 92–106 nm, we obtain a stress intensity factor value of 38–40 MPa m^{1/2} for steel with the given range of chemical analysis and applied heat treatment parameters.

Acknowledgement

The research was supported by the National Centre for Research and Development, Poland within the research project entitled “Reliable and durable in operation, modern railway rails with a length of 120 m, characterized by high mechanical properties, high resistance to cracking and modified microstructure of the material as a result of the modernization of the cooling process after rolling” – POIR.01.01.01-00-0438/18.

REFERENCES

1. Żak S., Bartyzel J., Kasprowicz J. Railway rails for heavy-duty tracks manufactured at Huta Katowice S.A. *Hutnik – Wiadomości Hutnicze*, 2001; 68(11): 404–408.
2. Bartyzel J., Liszka S. Research on the mechanism of wear of railway rails under conditions of high operational loads. Published materials of the 12th Scientific and Technical Conference Railway Roads 2003; 59–70.
3. European Standard EN 13674-1:2011+A1:2017 Railway applications – Track – Rail Part 1: Vignole railway rails 46 kg/m and above.
4. Guericke W., Heller W., Kasprowicz J., Weiße M. Verbesserte Bruchsicherheit von Schienen durch optimiertes Rollenrichten. *ETR Eisenbahntechnische Rundschau*, 2001; 50(9): 541–551.
5. Żak S., Woźniak D. Controlling the state of residual stresses in railway rails by modifying pass design of straightening rollers. *Arch. Metall. Mater.* 2023; 68(1), 57–70. <https://doi.org/10.24425/amm.2023.141473>
6. Żak S., Woźniak D. The influence of changes in roll pass design on the state of residual stresses in railway rails – summary. *Arch. Metall. Mater.* 2023; 68(2): 439–446. <https://doi.org/10.24425/amm.2024.147815>
7. Jericho E., Weiße M. Beitrag der Eigenspannungen zum Gebrauchsverhalten von Schienen”. Internationales Symposium Schienenfehler. 16–17 November 2000, Brandenburg an der Havel, 10–1 ÷ 10–9.
8. Urbńczyk E., Kasprowicz J. Steels intended for the production of railway rails. Rail conference, Warsaw 2005.
9. Kuziak R., Molenda R., Pietryka J., Zygmunt T., Potwora A. A new method of head hardening of rail profiles. *Hutnik – Wiadomości Hutnicze*, 2003; 70(2): 53–59.
10. Zygmunt T., Kasprowicz J., Żak S. Rail steel grade B1000 produced by ArcelorMittal Poland S.A.”. *Hutnik – Wiadomości Hutnicze*, 2013; 80(10): 686–691.
11. Żak S., Zygmunt T., Kasprowicz J., Kozera K. A new steel grade for grooved rails. *Technika Transportu Szynowego*, 2018; 3: 41–44.
12. Herian J., Aniołek K. Selected aspects of shaping of a rail steel microstructure and its influence on a resistance to abrasive wear. *Hutnik – Wiadomości Hutnicze*, 2007; 74(5): 251–255.
13. Christodoulou P., T Kermanidis A. T., Haide-menopoulos G.N. Fatigue and fracture behaviour of pearlitic Grade 900A steel used in railway applications. *Theoretical and Applied Fracture Mechanics* 2016, 83, 51–59. <https://doi.org/10.1016/j.tafmec.2015.12.017>
14. Li X.C., Ding H.H., Wang W.J., Guo J., Liu Q.Y., Zhou Z.R. Investigation on the relationship between microstructure and wear characteristic of rail materials. *Tribology International*, vol. 163, November 2021; 107152: 1–15.
15. ASTM E112-13. Standard Test Methods for Determining Average Grain Size. ASTM International 2014.
16. Fischer S., Harangozó D., Németh D., Kocsis B., Sysyn M., Kurhan D., & Brautigam, A, Investigation of heat-affected zones of thermite rail welding. *Facta Universitatis, Series: Mechanical Engineering*, 2023; 1–22.
17. Sevillano. J.G., 1979. On the yield and flow stress of

- lamellar pearlite. In *Strength of Metals and Alloys*. Pergamon, p. 819-824.
18. Ray K. K., Mondal D. The effect of interlamellar spacing on strength of pearlite in annealed eutectoid and hypoeutectoid plain carbon steels". *Acta Metallurgica et Materialia*, 1991; 39(10): 2201–2208, [https://doi.org/10.1016/0956-7151\(91\)90002-I](https://doi.org/10.1016/0956-7151(91)90002-I)
 19. Daymond. M.R., Priesmeyer. H.G. Elastoplastic deformation of ferritic steel and cementite studied by neutron diffraction and self-consistent modeling. *Acta materialia*. 2002; 50(6): 1613–1626.
 20. Modi O., Desmukh N., Mondal D., Jha A., Yegneswaran A., Khaira H. Effect of interlamellar spacing on the mechanical properties of 0.65% C steel. *Mater. Charact.* 2001; 46: 347–352. [https://doi.org/10.1016/S1044-5803\(00\)00113-3](https://doi.org/10.1016/S1044-5803(00)00113-3)
 21. Jabłońska M., Lewandowski F., Chmiela B., Gronostajski Z. Advanced Heat Treatment of Pearlitic Rail Steel. *Materials (Basel)*, 2023, Sep 27; 16(19): 6430, 1–16. <https://doi.org/10.3390/ma16196430>. PMID: 37834570; PMCID: PMC10573705.
 22. Grain Micrograph Processing and Analysis Tool by Mark Henning, https://www.mark-henning.de/mhm_about_eng.php
 23. PN-EN ISO 6506-1:2014-12. Metals – Brinell hardness measurement – Part 1: Test method.
 24. PN-EN ISO 6892-1:2020-05. Metals – Tensile test – Part 1: Room Temperature Test Method.
 25. ISO 12108:2018. Metallic materials – Fatigue testing – Fatigue crack growth method.
 26. ASTM E399-22 Standard Test Method for Linear-Elastic Plane-Strain Fracture Toughness of Metallic Materials, 2023.
 27. Inal. K., Lebrun. J.L., Belassel. M. Second-order stresses and strains in heterogeneous steels: Self-consistent modeling and X-ray diffraction analysis. *Met. Mater. Trans. A* 2004; 35: 2361–2369.
 28. Binder M., Mezhuyev V., Tschandl M., *IEEE Engineering Management Review*, 2023; 51(2). Predictive Maintenance for Railway Domain: A Systematic Literature Review, 120–140.
 29. Babachenko A., Podolskyi R., Kononenko A., Safronova E. Investigation of the influence of heat treatment modes of experimental steels for new generation railway rails on mechanical properties, *Fundamental and applied problems of ferrous metallurgy*, 2020; 34: 247–255, <https://doi.org/10.52150/2522-9117-2020-34-247-255>
 30. Ackert R.J., Nott M.A. Accelerated water cooling of railway rails in-line with the hot rolling mill. *Proc. Symp. Accelerated Cooling of Roled Steels*. Eds. Ruddle. G. E., Crawley. A. F. Winnipeg: Pergamon Press, 1987; 359–372.
 31. Sahay S.S., Mohapatra G., Totten G.E. Overview of pearlitic rail steels: accelerated cooling, quenching, microstructure and mechanical properties. *Journal of ASTM International*, 2009; 6: 1–26.
 32. Li G., Liu Z., Chen L., Hou X. Numerical calculation of the comprehensive heat transfer coefficient on the surface of rail in the spray cooling process. *Journal of Metallurgical Engineering*, 2015; 13–17.
 33. Snitko Iu.P., Galyamov A.Kh. The current state of rail production abroad. *Materials of the Jubilee Railway Commission 2002*, Novokuznetsk. 10–30.
 34. Macek W., Sampath D., Pejkowski Ł, Zak K. A brief note on monotonic and fatigue fracture events investigation of thin-walled tubular austenitic steel specimens via fracture surface topography analysis (FRASTA), <https://doi.org/10.1016/j.engfailanal.2022.106048>
 35. Macek W., Kopec M., Laska A., Kowalewski Z.L. Entire fracture surface topography parameters for fatigue life assessment of 10H2M steel. *Journal of Constructional Steel Research*, 2024, <https://doi.org/10.1016/j.jcsr.2024.108890>